Nuclear Instruments and Methods in Physics Research A 606 (2009) 517–522

Contents lists available at ScienceDirect

Nuclear Instruments and Methods in Physics Research A

journal homepage: www.elsevier.com/locate/nima

Photon flux monitor for a mono-energetic gamma ray source

R.E. Pywell *, O. Mavrichi, W.A. Wurtz, R. Wilson

Physics and Engineering Physics, University of Saskatchewan, 116 Science Place, Saskatoon, SK, Canada S7N 5E2

ARTICLE INFO

Article history:
Received 14 January 2009
Received in revised form
6 April 2009
Accepted 9 April 2009
Available online 23 April 2009

Keywords:
Photon counting
Flux monitor
Gamma rays
Beam intensity measurement

ABSTRACT

A novel photon flux monitor has been designed and tested for use at the Duke University High Intensity Gamma Source. The five-scintillator-paddle system detects recoil electrons and positrons from photoelectric, Compton and pair-production processes. It is designed to be insensitive to gain and detector threshold changes and is usable for photon energies above 5 MeV. It has been calibrated using direct counting with a NaI detector, and its efficiency has been shown to be well described by a GEANT4 simulation.

1. Introduction

The measurement of nuclear reaction cross-sections that are initiated by photons depends critically on an accurate measure of the number of photons incident on the reaction target. Sub-atomic physics has now reached the point where precision cross-section measurements are necessary to further our understanding of nuclear forces and the properties of fundamental particles. Considerable advances have been made in understanding the efficiency of nuclear particle detectors. However, for non-tagged photon sources, similar advances have not been made in the accuracy of photon flux measurements.

Many photon counting methods have been used in the past. For bremsstrahlung photon beams ionization chambers have commonly been used, for example the 'P2 chamber' [1]. Such devices rely on slow charge integration and so dead-time corrections are necessary since charge is collected while an acquisition system may be busy or stopped. Such dead-time corrections are difficult for modern high-count-rate experiments as they rely on a knowledge of the instantaneous photon flux which may or may not be constant.

Experiments that use photon tagging (for example Refs. [2–5]) count the number of post-bremstrahlung electrons striking a focal plane detector. This may be related to the number of photons reaching a target by applying a measured 'tagging efficiency.' The recoil electrons are counted using scalers which may be gated by the live time of the experiment, thus obviating the need for dead-time corrections.

The photon beam from the High Intensity Gamma Source (HIGS) is essentially mono-energetic but is not tagged. Direct counting of the number of photons using a high-efficiency detector (such as a NaI scintillator or lead-glass Cherenkov counter) is not possible because of the high photon fluxes expected. Therefore a direct counting detector with a low, accurately known efficiency is required.

Design criteria for such a monitor included the following: The efficiency of the monitor should be relatively low so that even at high photon fluxes (greater than 1×10^8 photons/s) counting could be accomplished using standard nuclear electronics. The monitor should be highly selective of interactions caused only by the primary photon beam, and thus insensitive to room background. The monitor should be weakly dependent on the gain of its components (e.g. drifts in the gain of a photomultiplier tube which in turn affects the energy level at which a discriminator fires). The monitor should have a prompt output that can be counted with a scaler that can be gated by the live time of an experiment. Because the monitor must remain in the photon beam during an experiment it must have low mass to reduce the background radiation produced by it that may interfere with a measurement.

Photon counting detectors, which employ the detection of recoiling photoelectrons, Compton scattered electrons, and pair-production electrons and positrons by plastic scintillators, have been used with some success at HIGS [6] and other facilities. However, these devices have not met all the above criteria with sufficient accuracy for high precision cross-section measurements. The device described in this paper is designed to meet the above criteria so that the measurement of photon fluxes, accurate to better than 2%, can be achieved.

* Corresponding author. Tel.: +1 306 966 6404; fax: +1 306 966 6400.
E-mail address: rob.pywell@usask.ca (R.E. Pywell).

0168-9002/$ - see front matter © 2009 Elsevier B.V. All rights reserved.
doi:10.1016/j.nima.2009.04.014

2. Flux monitor design

The photon flux monitor was designed with the aid of a simulation built using the GEANT4 [8] toolkit. Using the simulation it was possible to vary all parameters of the monitor to investigate the sensitivity of its efficiency to changes in such things as discriminator energy levels.

The final conceptual design of the monitor is illustrated in Fig. 1. Recoil electrons and positrons generated principally in the radiator are identified by a triple coincidence between the outputs of paddles 2, 3 and 4. An anti-coincidence with a veto paddle (paddle 1) is employed to remove charged particles generated upstream of the radiator.

The paddles are chosen to be thin, about 2 mm thick, to reduce their sensitivity to room background, which, in this environment, includes a fairly large flux of low-energy neutrons. Because the paddles are thin, the energy deposited by electrons and positrons passing through them will be approximately the same regardless of their energy. That is they will behave as approximately 'minimum ionizing' particles. Therefore, with a discriminator threshold set well below the minimum ionizing peak, the efficiency of each paddle for detecting such particles will be largely insensitive to gain shifts.

Some electrons and positrons that cause a triple coincidence in paddles 2–4 while having no hit in the veto can be generated from places other than in the radiator. In particular, in paddle 2 from places closest to the radiator where enough energy is deposited to be over the discriminator threshold, and in paddle 1 from places closest to the radiator where insufficient energy is deposited to be over the veto paddle threshold. Therefore the efficiency of the monitor does depend on the gain of paddles 1 and 2 more strongly than for the other paddles. However, the inclusion of a radiator greatly reduces this dependence since the majority of the minimum ionizing particles will be generated in it. The radiator material needs to be of sufficiently high atomic number so that the Compton, photoelectric and pair-production cross-sections are significantly higher than in scintillator material, while having low nucleon number so that background-producing nuclear reaction cross-sections are not too high. Aluminum was chosen as a reasonable compromise while being easy to obtain in rigid flat sheets. The overall efficiency of the monitor depends almost linearly on the thickness of the radiator.

Even with the presence of a radiator it is still important to know the gain, and hence the threshold levels, of paddles 1 and 2 if the efficiency of the monitor is to be modeled accurately by a calculation. The gain of all the paddles can found by noting the position of the minimum ionizing peak for an electron passing fully through the paddle. This is the reason for including the fifth paddle (paddle 0) in the design. A triple coincidence between paddles 0, 1 and 2 ensures that an electron passes fully through the veto paddle 1, and thus allows its gain to be determined.

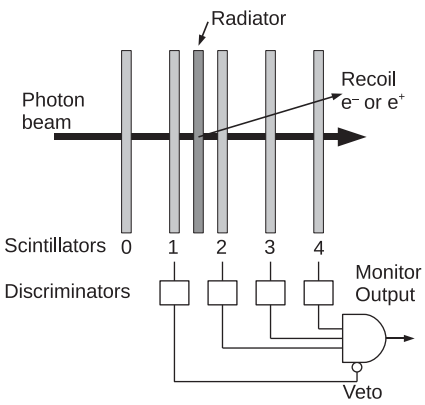

Fig. 1. Conceptual design of the photon flux monitor.

The simulation showed that the efficiency of the flux monitor depends weakly on construction dimensions such as the width and height of the paddles, the spacing between the paddles and the thickness of the scintillator material in the paddles. The strongest dependence was on the thickness of the aluminum absorber. An absorber thickness of 2 mm was chosen as being thick enough so that the monitor efficiency weakly depends on discriminator threshold levels while keeping the overall efficiency below about 2%. With this thickness a change of 10% in the discriminator level of paddle 1 or paddle 2 resulted in less that a 0.5% change in the efficiency of the monitor. The paddles were chosen to be BC-400 scintillators of, on average, 2.1 mm thick that were 10 cm high and 15 cm wide. With these dimensions the centering of a typically 1 in. (2.54 cm) diameter photon beam on the monitor is not critical.

Fig. 2 shows the predicted efficiency for the monitor as a function of energy. It can been seen that the monitor will be usable over a wide energy range.

An example of the calculated spectra from the paddles is shown in Fig. 3. Shown are the spectra for paddles 2, 3 and 4 when a triple coincidence between them and no signal from the veto paddle 1 is required. Two peaks can be seen in the spectra. The lower energy one corresponds to the minimum ionizing peak for a photoelectric or Compton electron. The higher energy one corresponds to the double minimum ionizing peak for an electron and positron pair passing through the paddle. The spectra are not influenced by the discriminator threshold for paddles 3 and 4 and is mostly above the threshold for paddle 2. Therefore small changes in gain will have little influence on the total number of counts.

The complete flux monitor was constructed using available components at the Department of Physics and Engineering Physics at the University of Saskatchewan. The 2.1 mm thick 15 cm $\times$10 cm BC-400 sheets are coupled to a phototube via adiabatic Lucite light guides attached to one of the 10-cm long edges. Philips XP2012, 10 stage, 39 mm diameter phototubes were used as these were readily available. The scintillator, light-guide and phototube assemblies are clamped in an aluminum frame so that the scintillator paddles are spaced 28.5 mm apart. Between paddles 1 and 2 a frame allows the mounting of various thickness radiators. For the tests described in this paper an aluminum radiator of thickness about 2.3 mm was used.

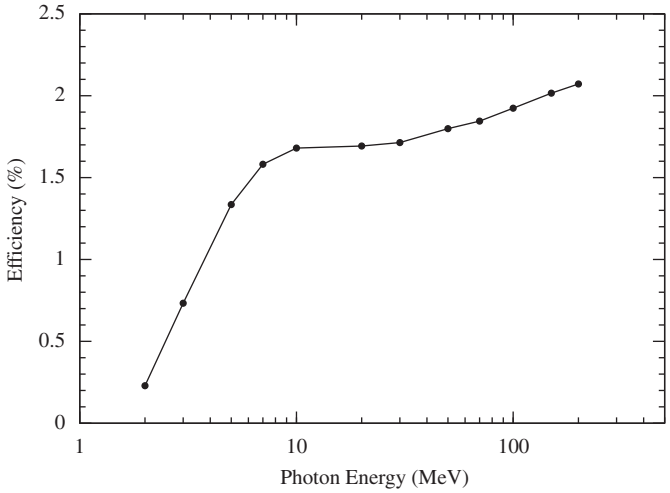

Fig. 2. The efficiency of the flux monitor, as calculated using the GEANT4 simulation, is plotted as a function of photon energy. The uncertainties in the calculated points are smaller than the plot symbols.

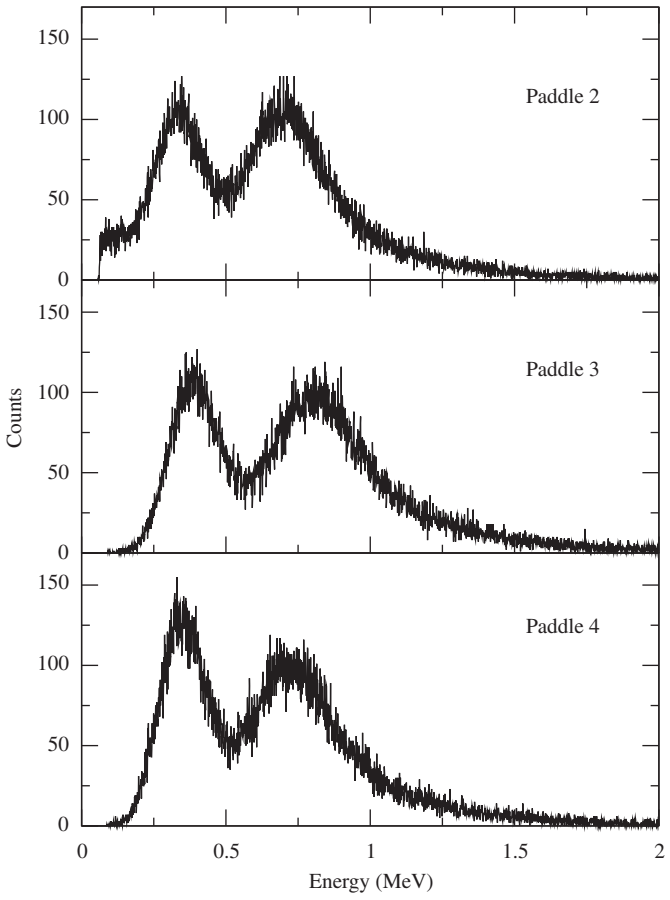

Fig. 3. Paddle spectra calculated from the simulation for a photon energy of 30 MeV. The spectra shown are for the condition of a triple coincidence between paddles 2, 3 and 4 and no hit in the veto paddle 1. Note that the energies of the minimum ionizing peaks for each paddle are at slightly different energies since the paddles have slightly different thicknesses.

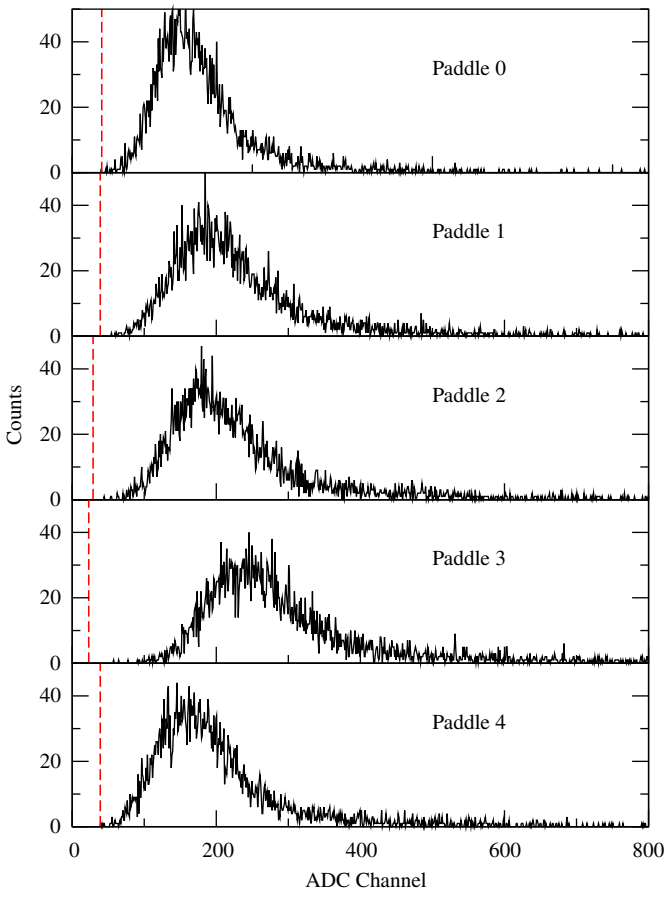

Fig. 4. The measured spectra from the five paddles due to cosmic ray muons when a coincidence between all five is required. Dashed lines show the threshold for each paddle.

3. Performance tests

After assembly an initial test was conducted using cosmic rays. The aluminum radiator was removed and the paddle assembly was placed on its side. A coincidence between all five paddles was required while the discriminator threshold for each paddle was set well above noise. The resulting spectra are shown in Fig. 4. The fact that the minimum ionizing peaks for the cosmic ray muons was well above the threshold levels indicated that the gain and resolution of the paddles are sufficiently good to operate in the manner necessary for the flux monitor.

In September and October of 2008 detailed tests and calibrations were carried out using the HIGS photon beam at four energies, 20, 25, 30 and 35 MeV. A schematic of the experimental arrangement used for these calibrations is shown in Fig. 5. A large NaI detector was moved into the beam downstream of the flux monitor, and the photon beam intensity was reduced by inserting copper absorbers into the beam line so that the NaI would be able to count individual photons. The effect of the copper absorbers has been studied in detail by the HIGS group [7]. Each attenuator is 8.0 cm thick and the attenuator assembly is located near the exit of the storage ring, almost 50 m from the primary collimator at the entrance to the gamma vault. This distance makes changes in the room background negligible when the attenuators are inserted. The shape of the spectrum seen in the NaI detector has been observed not to change when different numbers of copper absorbers are inserted. Because of the large distance between

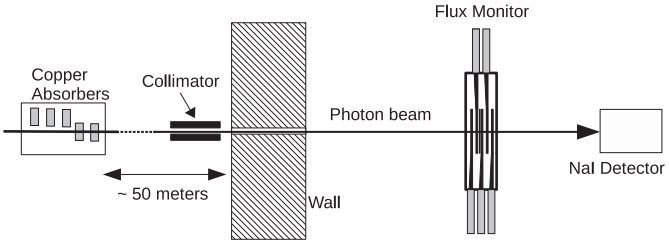

Fig. 5. A schematic of the experimental arrangement used to characterize the photon flux monitor (not to scale).

the copper attenuators and the primary collimator even photons scattered at very small angles in the copper attenuators are removed. This observation is supported by GEANT4 simulations which show that the NaI spectrum shape is unchanged when copper attenuators are inserted. The number of photons incident on the NaI detector was determined by integrating the NaI spectrum from about 9 MeV up. This removes the room background present at low energies, which is mostly natural radioactivity present even when the beam is off.

If we define, for the live time of the measurement, N_γ is the number of gamma rays incident on the monitor, N_m the number of measured gamma rays, i.e. the flux monitor counts, and N_{NaI} the number of gamma rays measured by the NaI detector. Then we can define, $\varepsilon_m = N_m/N_\gamma =$ the flux monitor efficiency, and $f_m =$

$1/\varepsilon_m$ = the flux monitor calibration factor, which are the quantities we desire. However, we do not measure N_γ directly but rather N_{NaI}.

Therefore, to begin with, we calculate, f'_m is the measured flux monitor calibration factor, using

$$f'_m = \frac{(N_{NaI} - B_{NaI}T_{live})}{(N_m - B_m T_{live})} \quad (1)$$

where T_{live} is the live time of the measurement, B_{NaI} the background rate in the integration region of the NaI spectrum (which was essentially zero for all runs), and B_m the background count rate of the flux monitor.

B_m was difficult to determine accurately. Because of the triple coincidence requirement in the flux monitor the major contribution to the background are cosmic rays incident at angles such that they pass through the three paddles while missing the veto paddle. In addition there is a contribution from the room background when random coincidences produce a count. Several measurements were made to estimate the background count rate. These measurements were necessarily made while the beam was off. It was found that different results were obtained depending on how long the beam had been off before the measurement was made. Therefore, the best estimate of the background rate was determined from a 1 h run taken just after the beam was turned off. Many measurements of f'_m were made at different photon rates, i.e. with different numbers of copper absorbers in place and different accelerator beam flux setups. It was found that at very low photon rates the value of f'_m depended strongly on the value of B_m used. The value of B_m that gave the same value of f'_m for all photon rates agreed with our experimental best estimate. Using this background rate the measured calibration factors for all photon rates, calculated using Eq. (1), agreed with each other within the errors of the measurements. However, due to the uncertainty in determining the background rate, only the measurements taken at flux monitor rates greater than 25 Hz were used. At these rates a factor of two uncertainty in B_m resulted in less than a 0.5% change in the measured flux monitor calibration factor for most measurements.

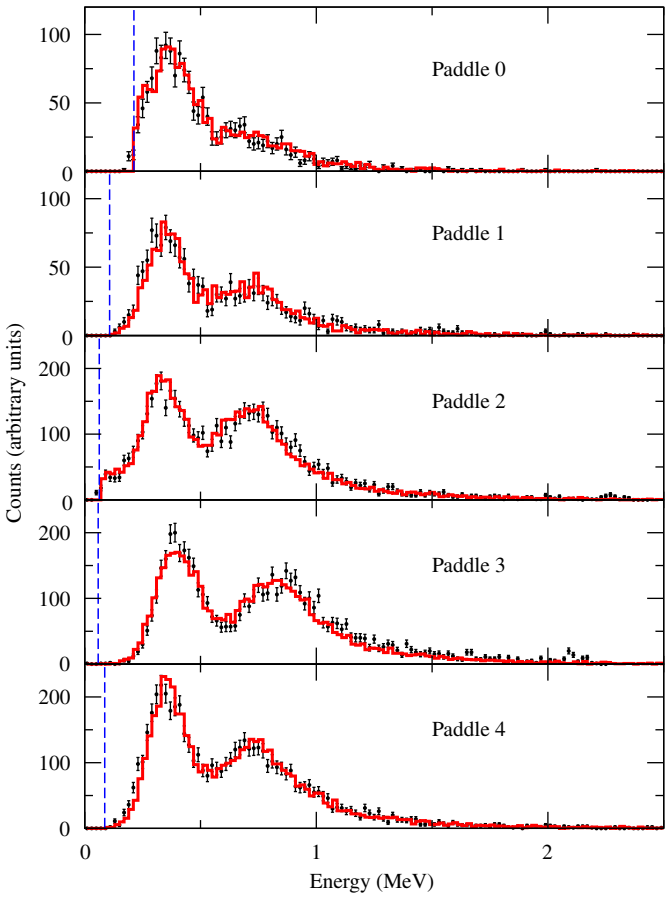

Fig. 6. Spectra from the five paddles in the flux monitor compared to the simulation for a beam energy of 25 MeV. The data points are measured spectra, the solid line is the GEANT4 simulation, and the vertical dashed lines show the location of the discriminator threshold. Spectra for paddles 2–4 are for a triple coincidence in anti-coincidence with the veto paddle 1. Spectra for paddles 0 and 1 are for a triple coincidence between paddles 0, 1 and 2 used for determining the gain of the veto paddle 1.

4. GEANT4 simulation

A simulation of the experimental arrangement including the flux monitor and the NaI detector has been developed using the GEANT4 [8] toolkit. The simulation includes all dimensions and materials in the flux monitor and the NaI detector and the relative positions of these two detectors and the primary collimator. The reasonable approximation of a uniform distribution of photons over the collimator opening was assumed. The simulation includes all relevant electromagnetic and hadronic interactions at these energies. This includes photon scattering and photon interactions producing recoil charged particles in all directions. From the simulation the spectrum from the flux monitor paddles and the NaI detector can be compared to the measured values. The simulation produces event by event data which allows the spectra, after applying the experimental thresholds and coincidence requirements, to be extracted.

During each experimental run a sample of the flux monitor spectra are recorded. An 'or' of all five discriminator outputs for the five paddles is used to generate a gate for an ADC connected to each paddle signal. A coincidence register also records which paddles were above its discriminator threshold.

The simulation is able to very well reproduce the spectra observed in the measurement as can be seen in Fig. 6. The figure shows the spectra from the five paddles of the flux monitor when a beam of energy 25 MeV passes through it. The paddles are labeled 0–4 with paddle 0 at the upstream end and the aluminum absorber is between paddles 1 and 2. A count from the monitor is determined by a triple coincidence between paddles 2, 3 and 4 in anti-coincidence with the veto paddle 1. In the figure the spectra for paddles 2–4 are for the normal condition for a flux monitor count i.e. in anti-coincidence with paddle 1. The spectra for paddles 0 and 1 are for the condition of a triple coincidence between paddles 0, 1 and 2, which is used to determine the gain of the veto paddle 1.

The energy calibration for each paddle was found by matching the single minimum ionizing peak (the lowest energy peak in each spectrum) to the energy determined from the simulation. The simulated spectrum was scaled by normalizing the integral in the energy range from 0.5 to 1.5 MeV to the integral of the measured spectrum. The energy resolution of the paddles was adjusted in the simulation to match the measured spectra. It can be seen from Fig. 6 that the shapes of the measured spectra are well reproduced by the simulation. The dashed blue lines in the figure show the discriminator thresholds for each paddle. These discriminator thresholds were determined from spectra incremented for a particular paddle with no coincidence requirement with other paddles but with the coincidence register bit set to indicate that paddle was above its discriminator threshold.

Table 1
Measured and calculated flux monitor calibration factors for the four beam energies.

Energy (MeV)	Absorption factor, c_{abs}	Calibration factor, f_m	Efficiency, ε_m (%)	Veto efficiency, ε_v (%)
20	1.0504	58.68 ± 0.50	1.703 ± 0.015	1.032 ± 0.005
25	1.0405	58.63 ± 0.50	1.705 ± 0.015	1.043 ± 0.005
30	1.0338	57.33 ± 0.51	1.745 ± 0.016	1.048 ± 0.005
35	1.0291	58.02 ± 0.43	1.723 ± 0.013	1.066 ± 0.005

Column 2 is the absorption correction factor calculated from the simulation. The uncertainty in this number is smaller than the precision quoted. Columns 3 and 4 are the measured calibration factor and efficiency after correction by the absorption factor. Column 5 is the probability of a hit in the veto (counter 1) calculated from the simulation as described in Section 5.

5. Absorption correction

The measured calibration factor f'_m is not equal to the true calibration factor f_m because not all gamma rays incident on the flux monitor reach, and are detected by, the NaI detector. The correction factor, defined by

$$c_{abs} = N_\gamma / N_{NaI} \tag{2}$$

is determined from the simulation for each energy.

The true calibration factor is then given by

$$f_m = c_{abs} f'_m. \tag{3}$$

The weighted mean of all measurements with flux monitor rates above 25 Hz was used to find the final true calibration factor. The results are summarized in Table 1.

The true calibration factor can also be calculated from the simulation provided all parameters of the flux monitor are known to sufficient precision. The most critical parameter in this calculation is the thickness of the aluminum absorber. The efficiency of the flux monitor is almost directly proportional to this thickness. Unfortunately this thickness is not known to sufficient precision. Micrometer measurements of the aluminum absorber thickness varied considerably. Therefore the thickness of the absorber in the simulation was adjusted until the average efficiency for the four energies agreed with the measured average efficiency. This was achieved with an absorber thickness of 2.297 mm which was within the range of the measurements. With this absorber thickness the average measured calibration factor agreed with the average calibration factor from the simulation to within less than 0.5%. The absorption correction factors quoted in Table 1 are calculated using this absorber thickness.

The measured and calculated calibration factors are plotted as a function of energy in Fig. 7.

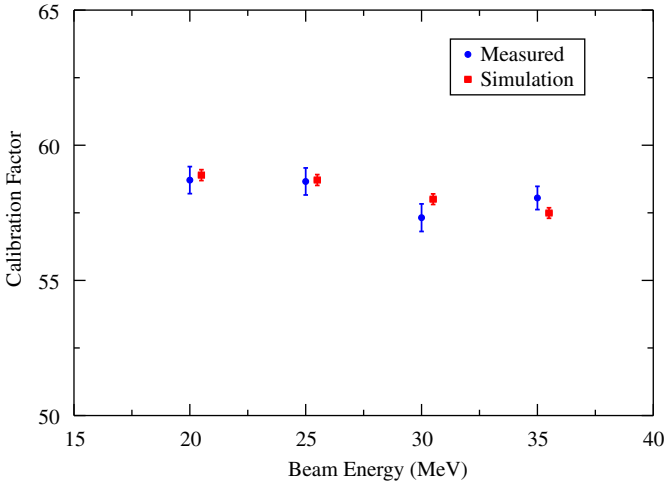

Fig. 7. Measured calibration factors and calculated calibration factors for the five-paddle flux monitor as a function of energy. For clarity the simulated values are offset by 0.5 MeV from the measured data points.

6. Rate correction

The HIGS beam is not a 100% duty factor photon beam. The photon beam comes in bunches at a rate of 5.58 MHz or about 180 ns apart. The dead-time of the flux monitor is of the order 60 ns (about the width of the veto generated by the veto paddle). Therefore photons arriving in separate bunches will always be counted by the scaler if they are detected by the flux monitor. However, more than one photon being detected in the flux monitor in a single bunch will be counted as only one.

The above calibration factors are measured at very low photon fluxes so that the probability of more than one photon being detected in a single bunch is extremely small. Therefore the measured efficiency, and the efficiency predicted by the GEANT4 simulation, where one photon at a time is simulated, is an absolute efficiency appropriate only at low rates. At high photon rates a correction for multiple hits in a bunch must be made.

The number of photons detected is reduced when two or more photons are detected in a single bunch and are counted as only one. A further reduction occurs when a photon is detected, but another photon in the same bunch causes a hit in the veto paddle, thus killing the detected photon.

Therefore in order to calculate the correction at high rates the probability that a photon hitting the flux monitor will cause a hit in the veto (paddle 1) is needed. This information can be obtained from the simulation. The results for the four energies under consideration are listed in column 5 of Table 1.

A full calculation of the probability of getting a count from the flux monitor in a single bunch is complicated and involves many terms. Fortunately a good approximation can found using the following simple argument.

We define, $N_h = \varepsilon_m N_\gamma =$ the number of hits on the flux monitor that have the potential to be counted. So then, $\mu_h = N_h/B =$ the average number of hits per bunch, where B is the number of accelerator bunches during the live time of a measurement. If $P_h(x_h, \mu_h)$ is the probability of x_h hits in a bunch from Poisson statistics then, since one or more hits will be counted as one, the probability of a count will be

$$P_h(x_h \geqslant 1, \mu_h) = 1 - P_h(0, \mu_h) = 1 - e^{-\mu_h}. \tag{4}$$

But this hit may be vetoed if another photon in the bunch causes a hit in the veto paddle. The probability that this occurs may be estimated as follows. Defining $\mu = N_\gamma/B =$ the average number of photons in a bunch, then $\mu - \mu_h =$ the average number of photons in a bunch that did not cause a detectable hit. If $\varepsilon_v =$ veto efficiency $=$ the probability that a photon causes a hit in the veto paddle, then, $\mu_v = (\mu - \mu_h)\varepsilon_v =$ the average number of those photons that cause a hit in the veto paddle. Therefore, from

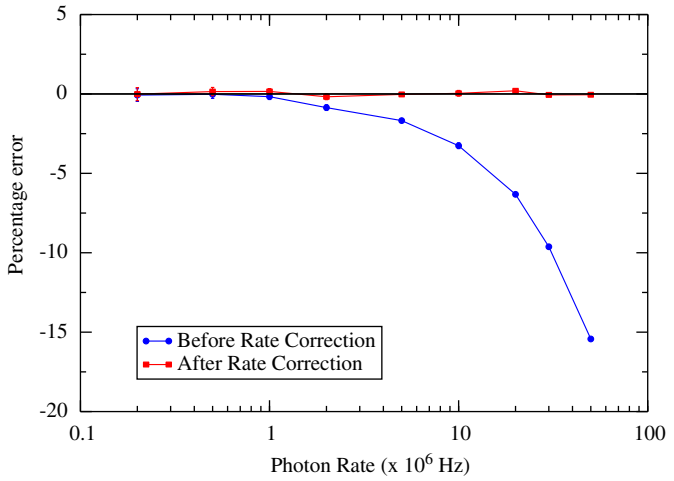

Fig. 8. The percentage error in the number of photons as a function of photon rate. The errors without applying a rate correction and after applying a correction are shown. Uncertainties in the simulation results are smaller than the size of the data points shown.

Poisson statistics, the probability that there is no hit in the veto paddle from these photons is

$$P_v(0,\mu_v) = e^{-\mu_v}. \tag{5}$$

Therefore the total number of counts from the flux monitor is

$$\begin{aligned} N_m &= BP_v(0,\mu_v)P_h(x_h \geqslant 1,\mu_h) \\ &= B\exp\left(-\varepsilon_v(1-\varepsilon_m)\frac{N_\gamma}{B}\right)\left(1-\exp\left(-\varepsilon_m\frac{N_\gamma}{B}\right)\right). \end{aligned} \tag{6}$$

This expression must be inverted to calculate N_γ from N_m. This is most easily done numerically. A first order expansion of Eq. (6) that can easily be inverted algebraically does not provide sufficient accuracy for photon rates over about 8×10^6 Hz.

The correctness of Eq. (6) for calculating N_γ was tested using Monte-Carlo simulations. In each simulation the number of photons in a bunch was selected using Poisson statistics for a given photon rate. Then, in one simulation, each of these photons was tracked using the GEANT4 code to determine if a hit occurred in that bunch. In a simpler, much faster simulation, the GEANT4 code was not used, but the known efficiencies for getting a normal hit from the monitor ε_m and for getting a hit in the veto ε_v were used to determine if a count from the monitor occurred in that bunch. Both simulations were found to give the same results.

In an actual experiment, both the total number of bunches B and the total number of flux monitor hits N_m during the live time of a measurement are recorded in scalers. Then, using the known values of the efficiencies ε_m and ε_v, the number of photons N_γ can be calculated from Eq. (6). This was tested, using the Monte-Carlo simulations described above, for a wide range of photon rates and the results are shown in Fig. 8. The figure shows the error in the calculated number of photons if the rate correction was ignored (i.e. if the number of photons was calculated by simply using $N_\gamma = N_m/\varepsilon_m$). Without a rate correction the calculated number of photons is too small, hence the negative error shown in the figure. After applying the rate correction it can be seen that Eq. (6) gives the correct number of photons to less 1%.

The error in N_γ depends on the uncertainties in N_m, ε_m and ε_v in the usual way,

$$\delta N_\gamma^2 = \left(\frac{\partial N_\gamma}{\partial N_m}\right)^2\delta N_m^2 + \left(\frac{\partial N_\gamma}{\partial \varepsilon_m}\right)^2\delta\varepsilon_m^2 + \left(\frac{\partial N_\gamma}{\partial \varepsilon_v}\right)^2\delta\varepsilon_v^2. \tag{7}$$

The coefficients in Eq. (7) can be estimated from a leading order approximation of Eq. (6). The results are

$$\frac{\partial N_\gamma}{\partial N_m} = \frac{1}{\varepsilon_m},\quad \frac{\partial N_\gamma}{\partial \varepsilon_m} = -\frac{N_m}{\varepsilon_m^2}\quad\text{and}\quad \frac{\partial N_\gamma}{\partial \varepsilon_v} = \frac{(1-\varepsilon_m)^2N_m^2}{\varepsilon_m^2 B}. \tag{8}$$

7. Stability

The photon flux monitor must have a stable efficiency over a wide range of photon intensities. Therefore the gain of each paddle must be stable so that the discriminator threshold level is stable. Although the monitor has been designed to be relatively insensitive to small changes in gain, it is important to monitor the gains during an experimental measurement. If changes in gain are observed a correction to the efficiency of the monitor can be calculated using the simulation.

As mentioned in Section 4, a pre-scaled sample of the spectra from each paddle is recorded during each experimental run. By observing the location of the single and double minimum ionizing peaks in these spectra the gain of each paddle may be determined and changes in this gain may be tracked.

During experimental runs at HIGS during 2008 at photon rates of up to 3×10^7 Hz no significant changes in gain were observed. This may be due in part to the fact that the count rate from the monitor is effectively limited by the bunch rate from the accelerator of 5.58 MHz, and therefore events in each paddle are, in general, at least 180 ns apart.

8. Conclusion

A photon flux monitor for the High Intensity Gamma Source at the Duke University Free-Electron Laser Facility has been developed. Its response is well characterized by a GEANT4 simulation. It has been shown to be stable over a wide range of photon intensities up to 3×10^7 photons/s. It may be accurately calibrated against a NaI detector at low photon rates and corrections needed at high photon rates are easily and accurately calculable. The monitor easily achieves its design goal of measuring the number of photons incident on it to at least the 2% accuracy needed for precision photonuclear reaction measurements.

Acknowledgments

The financial assistance of the Natural Science and Engineering Research Council of Canada is gratefully acknowledged. The authors wish to thank their colleagues, Sean Stave, Brad Sawatzky, Serpil Kucuker and members of the TUNL group at Duke University for their assistance in making the characterization measurements for the flux monitor.

References

[1] J.S. Pruitt, S.R. Domen, Determination of total X-ray beam energy with a calibrated ionization chamber, National Bureau of Standards Monograph 48, 1962.
[2] J.M. Vogt, R.E. Pywell, D.M. Skopik, E.L. Hallin, J.C. Bergstrom, H.S. Caplan, K.I. Blomqvist, W. Del Bianco, J.W. Jury, Nucl. Instr. and Meth. A 324 (1993) 198.
[3] I. Anthony, J.D. Kellie, S.J. Hall, G.J. Miller, J. Ahrens, Nucl. Instr. and Meth. A 301 (1991) 230.
[4] D.I. Sober, et al., Nucl. Instr. and Meth. A 440 (2000) 263.
[5] K. Hirose, et al., Nucl. Instr. and Meth. A 564 (2006) 100.
[6] R. Reynolds, APS Meeting Abstracts, DNP5P1061R, 2002.
[7] M.W. Ahmed, et al., TUNL Progress Report, vol. 46, 2007, p. 104.
[8] GEANT4 Collaboration, Nucl. Instr. and Meth. A 503 (2003) 250; GEANT4 Collaboration, IEEE Trans. Nucl. Sci. NS-53 (2006) 270.